





Sub-7 fs radially-polarized pulses by post-compression in thin fused silica plates

HUABAO CAO,^{1,2,*} ROLAND S. NAGYMIHALY,¹ NIKITA KHODAKOVSKIY,¹  VIKTOR PAJER,¹  JANOS BOHUS,¹  RODRIGO LOPEZ-MARTENS,^{1,3} ADAM BORZSONYI,¹ AND MIKHAIL KALASHNIKOV^{1,4}

¹ELI-ALPS, ELI-HU Non-Profit Ltd., Wolfgang Sandner u. 3, 6728 Szeged, Hungary

²Xi'an Institute of Optics and Precision Mechanics of CAS, 710119 Xi'an, China

³Laboratoire d'Optique Appliquée, CNRS, Ecole Polytechnique, ENSTA Paris, Institut Polytechnique de Paris, 181 chemin de la Hunière et des Joncherettes 91120 Palaiseau, France

⁴Max-Born-Institut for Nonlinear Optics and Short Pulse Spectroscopy, Max-Born-Strasse 2a, 12489 Berlin, Germany

*caohuabao@opt.ac.cn

Abstract: We experimentally demonstrate the post-compression of radially polarized 25 fs pulses at 800 nm central wavelength in a multiple thin plate arrangement for the first time, to the best of our knowledge. Sub-7 fs pulses with 90 μ J energy were obtained after dispersion compensation, corresponding to a compression factor of more than 3.5. Preservation of radial polarization state was confirmed by polarized intensity distribution measurements. Linear projections of the radially polarized pulses were also fully characterized in the temporal domain.

© 2021 Optical Society of America under the terms of the [OSA Open Access Publishing Agreement](#)

1. Introduction

Radially polarized beams are of great interest because of their exotic characteristics. Such beams can be tightly focused with a longitudinal electromagnetic field component [1], which is beneficial for many applications including laser micro-machining, particle acceleration, and plasmonic focusing [2–4]. Radially polarized beams composed of few-cycle pulses are more attractive for scientific applications, such as the generation of radially polarized isolated attosecond extreme ultraviolet pulses through high-order harmonic generation in gases [5] or low divergence MeV electron bunches via millijoule level laser-driven acceleration in micro-size parabolic plasma channels [6].

Nonlinear post-compression of radially polarized pulses in a hollow-core fiber (HCF) has been investigated both theoretically and experimentally [7,8]. Sub-3-cycle pulses with 60 μ J energy and radial polarization were achieved at 1.8 μ m central wavelength by using an HCF filled with krypton gas [8]. Efficient post-compression of linearly polarized pulses down to single-cycle duration has been demonstrated by spectral broadening through a sequence of multiple thin plates [9–11]. In contrast to the HCF compression technique, the multiple thin plate approach does not require sophisticated beam coupling arrangements or vacuum apparatus at energies in the few-hundred μ J range. Post-compression in a sequence of thin plates has not yet been investigated with driver pulses different from linear polarization.

Here, we present the first experimental results on nonlinear post-compression of radially polarized laser pulses using the multiple thin plate technique, to the best of our knowledge. Spectral broadening through 5 pieces of thin fused silica plates resulted in a sub-7 fs compressed pulse duration and 90 μ J pulse energy. Our experimental setup was realized in ambient air, by which no vacuum apparatus was utilized. The compressed radially polarized pulses were analyzed in both the temporal and spatial domains.

2. Experimental setup and results

Our experimental thin-plate post-compression setup was driven by the HF-100 frontend of the High Field Laser of ELI-ALPS, which is a hybrid chirped pulse amplification (CPA) system from Amplitude Technologies [Fig. 1]. The seed pulses are produced through supercontinuum generation from 500 fs pulses of an Yb:YAG thin-disk laser. The supercontinuum pulses are amplified in several parametric amplification stages, producing microjoule level output with high temporal contrast and 25 fs pulse duration around 800 nm central wavelength. These pulses are then amplified in a Ti:Sapphire-based CPA with two amplifier stages, resulting in 25 fs pulses with 8 mJ energy at 100 Hz repetition rate.

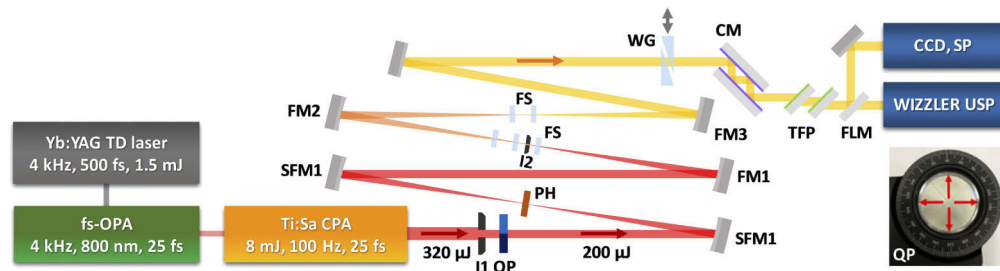


Fig. 1. Schematic of the pump source and multi-plate post-compression setup. TD stands for thin-disk, QP for a four-quadrant waveplate, SFM1 and SFM2 for focusing mirrors with focal length of 1 m for the spatial filter, PH for pinhole, I1 and I2 for irises, FM1, FM2 and FM3 for focusing mirrors of the nonlinear broadening stage, FS for fused silica plates, WG for wedge pair, CM for chirped mirrors, TFP is the rotatable thin film polarizer pair used in transmission mode, and FLM is a flip mirror. Inset: photo of the four-quadrant waveplate.

In order to prevent ionization in air at the focus within the setup, the pulse energy sent into the post-compression setup was limited to 320 μJ . The input pulses with linear polarization were sent through a 4-segment waveplate in order to transform the linearly polarized beam into a composite beam with four sections. A hard aperture located before the waveplate (I1 in Fig. 1) was used to tune the focal spot size (0.35 mm diameter at $1/e^2$ peak intensity level), while the pulse energy was measured to be 200 μJ just after the QP with a beam diameter of 8 mm. The polarization direction in each section of the composite beam gets rotated to different direction, indicated by the red arrow in the inset of Fig. 1. This composite beam can be further shaped into a radially polarized beam using a pinhole with diameter of 400 μm (I2 in Fig. 1) at the far field. The truncated beam was focused in air using a concave mirror with a focal length of 1 m. The spectral broadening induced by self-phase modulation (SPM) and self-steepening (SS) was achieved in a sequence of five thin fused silica plates of identical 150 μm thickness. The first three thin plates were positioned near the first beam focus, with 50 mm distance between the plates. Compression of the input pulses was optimized at the first thin plate by using the Dazzler (Fastlite) in the CPA system up to the fourth dispersion order. After propagating through the first three plates, the diverging beam was refocused by a second concave mirror with a focal length of 0.5 m. The last two thin plates were placed around the second focus, with 40 mm separation in order to obtain sufficiently high peak intensity for further spectral broadening. In contrast to the case of linear polarization, the angle of incidence on the plates was kept close to 0° to avoid polarization-dependent surface reflection losses. The spectrally broadened pulses were collimated by a third spherical mirror with a focal length of 0.5 m, then sent into the compressor consisting of a fused silica wedge pair, and a set of chirped mirrors with a dispersion of -40 fs^2 per bounce from 550 nm to 950 nm (Ultrafast Innovations GmbH). Within the optical path between the QP and the TFP, the radially polarized beam was always close to normal incidence

onto each reflective optics, i.e. reflective mirror or chirped mirror, to avoid the degradation of the polarization state introduced by reflection.

Linear polarization projections of the compressed pulses were characterized using a Wizzler USP (Fastlite) device placed after a rotatable thin film polarizer (TFP) used in transmission mode. Spectral broadening was also measured separately using a high bandwidth spectrometer (AvaSpec-3648, Avantes) for comparison. The spatial beam profile was characterized with a CCD camera (PIKE F-145C, Allied Vision).

Evaluation of the beam profiles after the TFP is necessary in order to verify that the radial polarization of the post-compressed pulses is preserved, i.e. the newly generated frequency components possess the same polarization state. The beam profiles measured by a CCD camera are shown in Fig. 2 when a spatial filter was employed before the QP (shown in Fig. 1). One can see in Fig. 2(a) the beam without the TFP in the beam path, which resembles the doughnut intensity distribution. The beam profiles after the TFP are shown in Fig. 2(b)-(d). A double-lobe structure can be observed when the TFP is aligned at three different angles, i.e. 0° , 90° and 45° with respect to the incident (horizontal) plane of polarization [12].

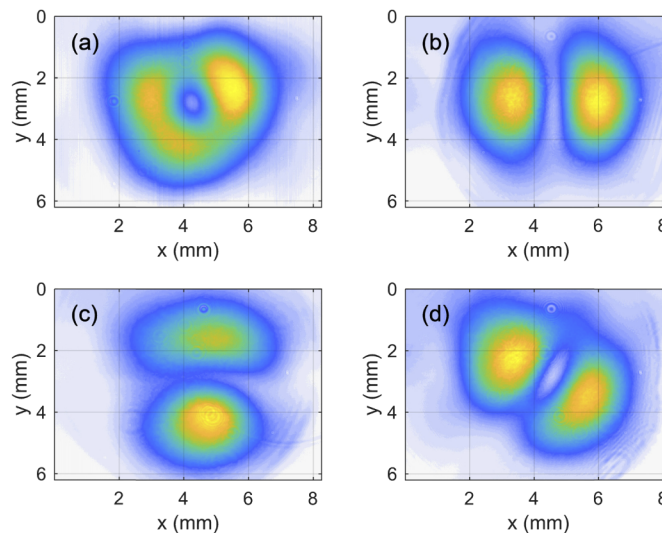


Fig. 2. Spectrally broadened beam profiles measured with a spatial filter located before the four-segment waveplate: (a) before the TFP, and after TFP aligned horizontally (b), vertically (c), and at 45° (d).

The beam quality of the post-compressed pulses was highly dependent on the input beam quality on the QP. This is illustrated in Fig. 3: here, when the spatial filter before the QP is removed, the doughnut intensity profile without TFP and the double-lobe structures measured with TFP all became more asymmetric compared to the profiles shown in Fig. 2. In addition to that, high order spatial mode components other than the radially polarized ones emerge and continuously evolve during the nonlinear propagation, manifested by the complex intensity distribution adjacent to the main beam. It is worth mentioning that the use of a spatial filter before the QP introduced modulation at the blue wing of the broadened spectrum because of the ionization of the air in the focus of the spatial filter [13], which can be avoided by using concave mirrors of longer focal length in the spatial filter if there is enough space on the optical table. Therefore, the characterization of the spectral and temporal properties of the compressed pulses was performed with the pulses depicted in Fig. 3 to exclude the air-ionization induced effect.

Figure 4 compares the broadened spectra measured after the TFP at different orientations compared to the input spectrum on a logarithmic scale. The spectra measured at different

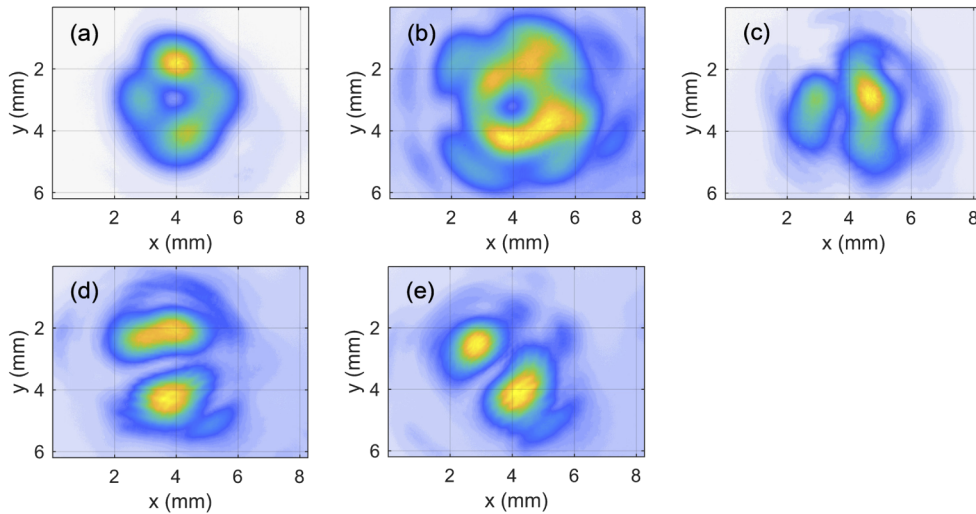


Fig. 3. Beam profiles of post-compressed pulses measured when removing the spatial filter located before the four-segment waveplate: (a) without thin plates, (b) with thin plates. Spectrally broadened beam profiles after the TFP aligned: (c) horizontally, (d) vertically, (e) at 45° , respectively.

polarization directions possess very similar features, especially at the red and blue wings, and the moderate difference is attributed to the spatial intensity distribution imperfections of the input beam profile [Fig. 3(a)]. A broadening factor of more than 3.5 was achieved for all TFP orientations. The red side of the spectrum at 950 nm and the blue side at 550 nm at the normalized intensity level of 10^{-3} is cut by the finite bandwidth of the chirped mirrors (indicated by grey dashed lines in Fig. 4) used for temporal compression before the TFP. The stronger spectral broadening towards the blue side is characteristic for SS. It also needs to be mentioned, that a non-negligible spectral broadening is already visible without the plates (Input, Fig. 4), which is due to SPM generated in air in the close vicinity of the first focus.

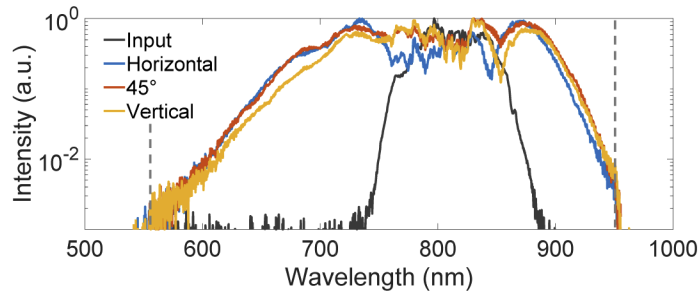


Fig. 4. Measured broadened spectra with TFP aligned horizontally (blue line), 45° (orange line) and vertically (yellow line). The grey line represents the spectrum without thin plates inserted in the beam path, measured at the same position. The vertical grey dashed lines indicate the bandwidth limitations of the chirped mirrors.

Temporal characterization of the linear projections of the radially polarized pulses was performed after the TFP and an aperture. The latter was used to select out the core area of the beam. Figure 5 shows the spectral intensity distribution (solid blue lines) and the spectral phase (solid orange lines) retrieved by Wizzler, where the orientation of the polarizer was tuned to be

horizontal, vertical and 45°, respectively. The corresponding pulse durations are 6.9 fs, 6.8 fs and 6.5 fs FWHM, which were calculated based on the retrieved spectral intensity and phase [Fig. 5(d)]. Reliability of the Wizzler measurement was verified with measurements done with the separate spectrometer [gray dashed lines in Fig. 5(a)-(c)], which are comparable to the ones retrieved from the Wizzler measurement.

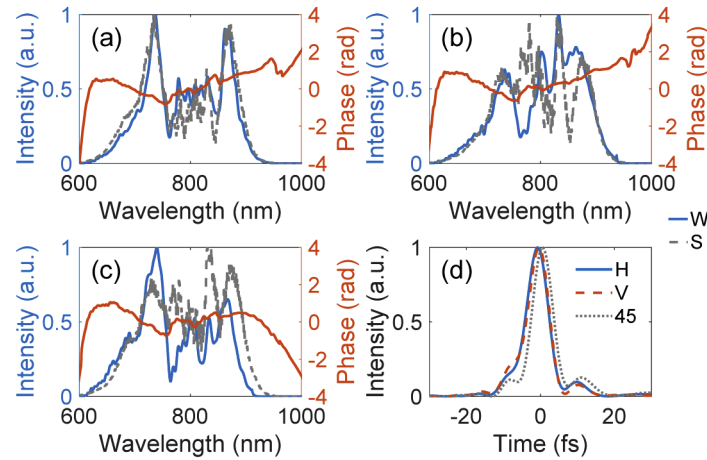


Fig. 5. Results of temporal characterization of the post-compressed pulses after the TFP for three polarization directions: horizontal (a), vertical (b) and 45° (c). Spectral intensity (W) and phase retrieved from the Wizzler USP measurement (blue and orange lines respectively). Spectral intensity measured by the separate Avantes spectrometer (gray dashed lines, S). Temporal intensity profile of the retrieved pulses (d) for the horizontal (H), vertical (V) and 45° (45) polarization directions.

The pulse energy after compression was measured to be 90 μJ , indicating an overall transmission efficiency of about 45%. Post-compression of linearly polarized pulses with a thin plate arrangement is known for its high transmission, because the reflection losses are kept low by setting the angle of incidence on the plates close to the Brewster angle. In our experiment the beam was normally incident on the thin plates, introducing high Fresnel losses due to the uncoated plate surfaces. The transmission efficiency is 70.6% after propagating through the 5 thin plates, and additionally the pinhole aperture at the first focus further removed part of the energy from the pulses to improve the beam quality. Therefore, the pulse energy dropped to 120 μJ before the temporal compression setup and decreased further to 90 μJ after compression with an aperture before the energy meter to exclude the exterior part of the beam.

3. Simulation results

To get a deeper understanding of the spectral broadening process we performed numerical simulations using a 3 + 1D code, in which beam propagation (diffraction), SPM, self-focusing, SS and dispersion of the nonlinear material are included. The details of the simulation can be found in [14] and the nonlinear refractive index of fused silica was set to $2.3 \cdot 10^{-16} \text{ cm}^2/\text{W}$ [15]. The spatio-temporal beam profile at the first thin plate was obtained numerically by assuming a Gaussian input spectrum, while taking a flat-top beam profile after the hard aperture. The peak intensity at the first plate was found to be $9.4 \text{ TW}/\text{cm}^2$, obtained from numerical simulation and we assumed an ideal radially polarized beam profile to simplify the simulation. The results are shown in Fig. 6, where it can be seen in Fig. 6(a) that the B-integral in each thin plate is already high enough to create a background around the main beam (the intensity distribution beyond $\pm 0.25 \text{ mm}$). This also explains the energy loss when the energy was measured after compression

(before the Wizzler). The spectrum at the position of maximum intensity is compared to the one measured after the 5th plate in Fig. 6(b). The simulated spectrum agrees well with measurement.

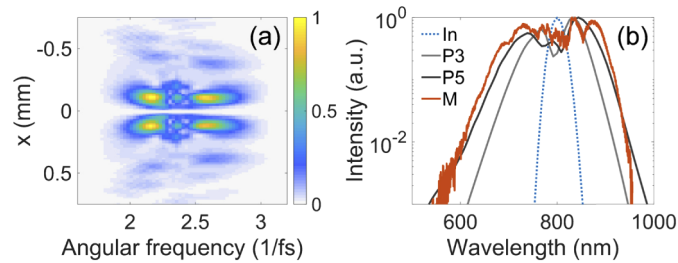


Fig. 6. Simulated spatio-spectral intensity distribution with the experimental parameters after the 5th thin plate (a). Comparison between the simulated spectra (b) after three thin plates (P3), five plates (P5), fundamental (In), and measured after five plates (M).

4. Discussion

The duration of the radially polarized pulse can be further shortened by introducing higher nonlinear phase, via increasing the thickness of the thin plates. However, the larger B-integral accumulated in a single plate will spread the pulse energy away from the central spatial lobe and therefore enhance the spatio-spectral couplings. The alternative is to increase the number of thin plates, however, it is not straightforward for radially polarized pulses due to the increased reflection losses at normal incidence. The spatial Kerr effect for a linearly polarized pulse with Gaussian spatial profile results in self-focusing, which is helpful to maintain a quasi-constant intensity for effective nonlinear broadening in several consecutive thin plates without using additional focusing elements. However, the spatial Kerr effect for radially polarized pulses would rather decrease the annular diameter of the doughnut intensity profile, while the outer diameter of the doughnut profile is increased due to the diffraction effect. Therefore, additional focusing optics are needed to provide sufficient intensity to achieve noticeable spectral broadening. This is one of the reasons, why the radially polarized pulses were focused twice in our arrangement. Moreover, the multiple focusing configuration can serve as a quasi-waveguide, which is beneficial both for the mode preservation and the transmission efficiency. The refocusing can be implemented with protected metallic coatings (e.g. protected silver mirrors), which feature broad reflection bandwidth and low dispersion [16].

To overcome the reflection losses due to working at normal incidence, anti-reflective coatings can be applied. For instance, a silica sol-gel coating or single dielectric layer coating could be applied to suppress the Fresnel losses from the interfaces. The damage threshold of nano-porous anti-reflective silica thin film coatings for pulses of 35 fs duration already reaches 3 J/cm² [17], while according to a recent experimental study, the damage threshold of a single-layer anti-reflective coating is 0.8 J/cm² for 8 fs pulses [18]. Therefore, the anti-reflective coating could withstand peak intensities around 10 TW/cm² for the configuration used in our work. The thermal effect on the damage threshold at 100 Hz repetition rate can be considered negligible. On the other hand, if the repetition rate is increased to 100s of kHz, the thermally assisted damage mechanisms will decrease the damage threshold of the coatings [19]. This problem can be greatly mitigated by continuously rotating or translating the thin plates.

The HCF post-compression technique has shown great potential to routinely provide few-cycle linearly polarized pulses by nonlinear spectral-broadening, by which single-cycle pulse duration is possible to achieve [20,21]. Pulse energy has been scaled up to a-few tens of millijoule [22], and the average power reaches beyond 300 W by active cooling [23] with this technique now. The application to radially polarized beams has also been studied [8]. Regarding the technique of

multiple thin plates, millijoule level linearly polarized pulses in the single-cycle regime have already been demonstrated, and no physical obstacles are foreseeable in achieving single-cycle pulse radially polarized pulses with similar energy. The pulse energy can be scaled up with larger setups, similar as the HCF technique. Considering the average power, solid plates with low absorption and good thermal characteristics (e.g. fused silica) can be employed for high average power systems. For instance, post-compression at average power of 300 W has been realized based on fused silica plates with 12 mm thickness [24]. Therefore, the technique based on multiple thin plates can perform comparably to HCF from the aspects of pulse energy, pulse duration and average power. In addition, multiple thin plates schemes are generally simpler compared to the HCF technique and can potentially provide higher transmission efficiency when adequate anti-reflective coatings are used. Spatio-temporal couplings are, on the other hand, of concern in case of the multiple thin plate method, as these highly dependent on the spatial intensity distribution of the initial pulses. High energy pulses in the Joule level could be spectrally broadened in thin plates in the near field, especially using Super-Gaussian beam profiles to keep the broadening uniform across the beam cross-section.

5. Summary

In conclusion, we have experimentally demonstrated the feasibility of the multiple thin plate post-compression of radially polarized 25 fs pulses around 800 nm wavelength and achieved sub-3-cycle post-compressed pulse durations, corresponding to more than 3.5 times pulse shortening. The pulse duration can be further shortened towards the single-cycle with additional thin plates and focusing optics, while the energy loss from the Fresnel reflection on the thin plate surfaces can be greatly reduced using high damage threshold anti-reflective coatings. The setup of this technique is simple and adaptable to single-cycle millijoule pulses with high average power. Upscaling of the pulse energy to multi-mJ level seems feasible by enlarging the setup and by housing the experiment under vacuum in order to mitigate nonlinear effects in air. The experimental results of this work provide preliminary demonstration of the generation of few-cycle radially polarized pulses and further investigations are scheduled to improve the performance. This technique may provide a potential route to generate few-cycle radially polarized pulses for the study of high-field light-matter interactions.

Funding. ELI-ALPS (GINOP-2.3.6-15-2015-00001); Science and Technology Program of Xi'an (No. 202005YK01); Nemzeti Tehetség Program (NTP-NFTÖ-20-B-0058).

Acknowledgments. The authors thank Jérôme Faure for the loan of the four-segment waveplate and Amplitude Technologies for the support on the laser source. The ELI-ALPS project (GINOP-2.3.6-15-2015-00001) is supported by the European Union and co-financed by the European Regional Development Fund.

Disclosures. The authors declare no conflicts of interest.

References

1. R. Dorn, S. Quabis, and G. Leuchs, "Sharper focus for a radially polarized light beam," *Phys. Rev. Lett.* **91**(23), 233901 (2003).
2. C. Hnatovsky, V. G. Shvedov, N. Shostka, A. V. Rode, and W. Krolikowski, "Polarization-dependent ablation of silicon using tightly focused femtosecond laser vortex pulses," *Opt. Lett.* **37**(2), 226–228 (2012).
3. L. Wong and F. X. Kärtner, "Direct acceleration of an electron in infinite vacuum by a pulsed radially-polarized laser beam," *Opt. Express* **18**(24), 25035–25051 (2010).
4. Q. Zhan, "Evanescent Bessel beam generation via surface plasmon resonance excitation by a radially polarized beam," *Opt. Lett.* **31**(11), 1726–1728 (2006).
5. C. Hernández-García, A. Turpin, J. S. Román, A. Picón, R. Drevinskas, A. Cerkauskaitė, P. G. Kazansky, C. G. Durfee, and IJ Sola, "Extreme ultraviolet vector beams driven by infrared lasers," *Optica* **4**(5), 520–526 (2017).
6. M. Wen, Y. I. Salamin, and C. H. Keitel, "Electron acceleration by a radially-polarized laser pulse in a plasma micro-channel," *Opt. Express* **27**(2), 557–566 (2019).
7. Y. Zhao, D. Wang, R. Zhao, and Y. Leng, "Energetic radially polarized few-cycle pulse compression in gas-filled hollow-core fiber," *Opt. Express* **25**(17), 20866–20876 (2017).
8. F. Kong, H. Larocque, E. Karimi, P. B. Corkum, and C. Zhang, "Generating few-cycle radially polarized pulses," *Optica* **6**(2), 160–164 (2019).

9. C. Lu, Y. Tsou, H. Chen, B. Chen, Y. Cheng, S. Yang, M. Chen, C. Hsu, and A. Kung, "Generation of intense supercontinuum in condensed media," *Optica* **1**(6), 400–406 (2014).
10. P. He, Y. Liu, K. Zhao, H. Teng, X. He, P. Huang, H. Huang, S. Zhong, Y. Jiang, S. Fang, X. Hou, and Z. Wei, "High-efficiency supercontinuum generation in solid thin plates at 0.1 TW level," *Opt. Lett.* **42**(3), 474–477 (2017).
11. M. Seo, K. Tsendsuren, S. Mitra, M. Kling, and D. Kim, "High-contrast, intense single-cycle pulses from an all thin-solid-plate setup," *Opt. Lett.* **45**(2), 367–370 (2020).
12. C. F. Phelan, J. F. Donegan, and J. G. Lunney, "Generation of a radially polarized light beam using internal conical diffraction," *Opt. Express* **19**(22), 21793–21802 (2011).
13. B. Beaupaire, D. Guénot, A. Vernier, F. Böhle, M. Perrier, A. Jullien, R. Lopez-Martens, A. Lifschitz, and J. Faure, "Limitations in ionization-induced compression of femtosecond laser pulses due to spatio-temporal couplings," *Opt. Express* **24**(9), 9693–9705 (2016).
14. H. Cao, R. S. Nagymihaly, V. Chvykov, N. Khodakovskiy, and M. Kalashnikov, "Multipass-cell-based post-compression of radially and azimuthally polarized pulses to the sub-two-cycle regime," *J. Opt. Soc. Am. B* **36**(9), 2517–2525 (2019).
15. N. Garejev, G. Tamošauskas, and A. Dubietis, "Comparative study of multioctave supercontinuum generation in fused silica, YAG, and LiF in the range of anomalous group velocity dispersion," *J. Opt. Soc. Am. B* **34**(1), 88–94 (2017).
16. P. Balla, A. Bin Wahid, I. Sytcevic, C. Guo, A. Viotti, L. Silletti, A. Cartella, S. Alisauskas, H. Tavakol, U. Grosse-Wortmann, A. Schönberg, M. Seidel, A. Trabattori, B. Manschwetus, T. Lang, F. Calegari, A. Couairon, A. L'Huillier, C. L. Arnold, I. Hartl, and C. M. Heyl, "Postcompression of picosecond pulses into the few-cycle regime," *Opt. Lett.* **45**(9), 2572–2575 (2020).
17. M. Khatiri, F. Hajiesmaeilbaigi, H. Razaghi, A. Panahpour, and A. Bananej, "The effect of different drying methods on band gap energy and femtosecond LIDT of nano-porous anti-reflective silica thin films," *Opt. Quantum Electron.* **50**(8), 312 (2018).
18. N. Talisa, A. Alshafey, M. Tripepi, J. Krebs, A. Davenport, E. Randel, C. S. Menoni, and E. A. Chowdhury, "Comparison of damage and ablation dynamics of multilayer dielectric films initiated by few-cycle pulses versus longer femtosecond pulses," *Opt. Lett.* **45**(9), 2672–2675 (2020).
19. B. J. Nagy, L. Gallais, L. Vámos, D. Oszetzky, P. Rácz, and P. Dombi, "Direct comparison of kilohertz- and megahertz-repetition-rate femtosecond damage threshold," *Opt. Lett.* **40**(11), 2525–2528 (2015).
20. E. C. Jarque, J. S. Roman, F. Silva, R. Romero, W. Holgado, M. A. Gonzalez-Galicia, B. Alonso, I. J. Sola, and H. Crespo, "Universal route to optimal few- to single-cycle pulse generation in hollow-core fiber compressors," *Sci. Rep.* **8**(1), 2256 (2018).
21. M. Ouillé, A. Vernier, F. Böhle, M. Bocoum, A. Jullien, M. Lozano, J. Rousseau, Z. Cheng, D. Gustas, A. Blumenstein, P. Simon, S. Haessler, J. Faure, T. Nagy, and R. Lopez-Martens, "Relativistic-intensity near-single-cycle light waveforms at kHz repetition rate," *Light: Sci. Appl.* **9**(1), 47 (2020).
22. G. Fan, P. A. Carpeggiani, Z. Tao, E. Kaksis, T. Balčiūnas, G. Coccia, V. Cardin, F. Légaré, B. E. Schmidt, and A. Baltuška, "TW-Peak-Power Post-Compression of 70-mJ pulses from an Yb Amplifier," in *Conference on Lasers and Electro-Optics, OSA Technical Digest* (Optical Society of America, 2019), paper SW4E.1.
23. T. Nagy, S. Hädrich, P. Simon, A. Blumenstein, N. Walther, R. Klas, J. Buldt, H. Stark, S. Breitskopf, P. Jójárt, I. Seres, Z. Várallyay, T. Eidam, and J. Limpert, "Generation of three-cycle multi-millijoule laser pulses at 318 W average power," *Optica* **6**(11), 1423–1424 (2019).
24. J. Weitenberg, A. Vernaleken, J. Schulte, A. Ozawa, T. Sartorius, V. Pervak, H. Hoffmann, T. Udem, P. Russbüdt, and T. W. Hänsch, "Multi-pass-cell-based nonlinear pulse compression to 115 fs at 7.5 μ J pulse energy and 300 W average power," *Opt. Express* **25**(17), 20502–20510 (2017).